

AD-A036 918

LITTLE (ARTHUR D) INC CAMBRIDGE MASS
HIGH PRESSURE FURNACE GROWTH OF MERCURY CADMIUM TELLURIDE.(U)
AUG 76 J M PARRY

F/G 17/5

F33615-73-C-5155

UNCLASSIFIED

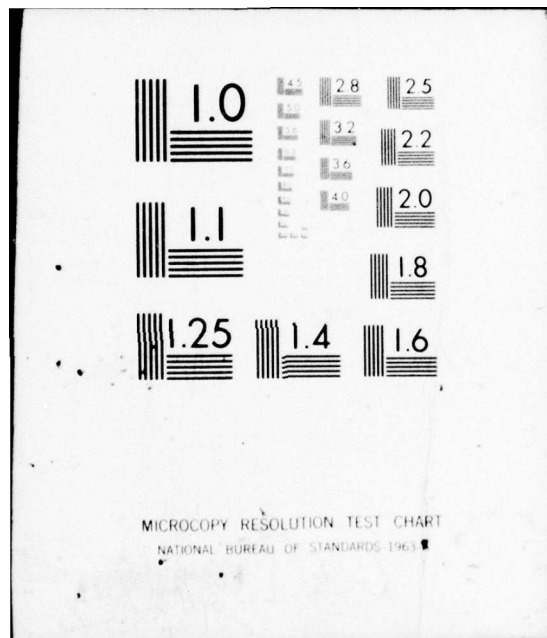
ADL-C-75953

AFML-TR-76-157

NL

1 OF 1
AD
A036918





ADA 036918

AFML-TR-76-157

(12) *J*

HIGH PRESSURE FURNACE GROWTH OF MERCURY CADMIUM TELLURIDE

ARTHUR D. LITTLE, INC.
25 ACORN PARK
CAMBRIDGE, MASS. 02140

AUGUST 1976

TECHNICAL REPORT AFML-TR-76-157
FINAL REPORT FOR PERIOD JUNE 1973 - APRIL 1976

Approved for public release; distribution unlimited

DDC
RECEIVED
MAR 15 1977
A
J

AIR FORCE MATERIALS LABORATORY
AIR FORCE WRIGHT AERONAUTICAL LABORATORIES
AIR FORCE SYSTEMS COMMAND
WRIGHT-PATTERSON AIR FORCE BASE, OHIO 45433

NOTICE

When Government drawings, specifications, or other data are used for any purpose other than in connection with a definitely related Government procurement operation, the United States Government thereby incurs no responsibility nor any obligation whatsoever; and the fact that the government may have formulated, furnished, or in any way supplied the said drawings, specifications, or other data, is not to be regarded by implication or otherwise as in any manner licensing the holder or any other person or corporation, or conveying any rights or permission to manufacture, use, or sell any patented invention that may in any way be related thereto.

This technical report has been reviewed and is approved for publication.

Robert Hickmott
Signature
Project Engineer

FOR THE COMMANDER

W D U Frederick
WILLIAM G. D. FREDERICK, Chief
Laser & Optical Materials Branch
Electromagnetic Materials Division
Air Force Materials Laboratory

Copies of this report should not be returned unless return is required by security considerations, contractual obligations, or notice on a specific document.

UNCLASSIFIED

SECURITY CLASSIFICATION OF THIS PAGE (When Data Entered)

19 REPORT DOCUMENTATION PAGE		READ INSTRUCTIONS BEFORE COMPLETING FORM
1. REPORT NUMBER 18 AFML-TR-76-157	2. GOVT ACCESSION NO.	3. RECIPIENT'S CATALOG NUMBER 9
4. TITLE (and Subtitle) 6 High Pressure Furnace Growth of Mercury Cadmium Telluride	5. TYPE OF REPORT & PERIOD COVERED Final Technical Report, June 1973—April 1976	
7. AUTHOR(s) 10 John M. Parry	8. CONTRACT OR GRANT NUMBER(s) 15 F33615-73-C-5155 <i>new</i>	6. PERFORMING ORG. REPORT NUMBER C75953
9. PERFORMING ORGANIZATION NAME AND ADDRESS Arthur D. Little Inc. 25 Acorn Park Cambridge, MA 02140	10. PROGRAM ELEMENT, PROJECT, TASK AREA & WORK UNIT NUMBERS 61101F, 62102F 7371, 737102 ILIR0039	11. REPORT DATE 11 August 1976
11. CONTROLLING OFFICE NAME AND ADDRESS Laser and Optical Materials Branch, AFML/LPO Air Force Materials Lab Wright-Patterson Air Force Base, OH 45433	12. NUMBER OF PAGES 56	13. SECURITY CLASS. (of this report) Unclassified
14. MONITORING AGENCY NAME & ADDRESS (if different from Controlling Office) 14 ADL-C-75953	15a. DECLASSIFICATION/DOWNGRADING SCHEDULE	16. DISTRIBUTION STATEMENT (of this Report) Approved for public release; distribution unlimited 12 6 pp.
16. DISTRIBUTION STATEMENT (of this Report) 16 7371, ILIR	17. SUPPLEMENTARY NOTES 17 02, ≠ 00	19. KEY WORDS (Continue on reverse side if necessary and identify by block number) Mercury Cadmium Telluride High Pressure Furnace Growth Infrared Sensors Phase Diagram
20. ABSTRACT (Continue on reverse side if necessary and identify by block number) This program involved the preparation of mercury cadmium telluride (HgCdTe) for infrared detectors using high pressure furnace technology. The principal difference between this approach and other techniques is that there is no requirement to seal the ampoule; the mercury vapor present during compounding and recrystallization is contained by the high pressure of inert gas in the furnace coupled with condensation of mercury vapor in the cool neck of the ampoule. The advantage of the method is that, unlike sealed ampoule techniques, the pressure		

208850

Handwritten signature/initials

UNCLASSIFIED

SECURITY CLASSIFICATION OF THIS PAGE(When Data Entered)

can be varied during preparation and recrystallization and there can be direct access to the melt for temperature measurement.

In all thirty ingots were prepared. The manufacturing variables included the rate and technique of solidification, furnace configuration, and times and temperatures during the recrystallization step. Initially ~~we encountered~~ difficulties in obtaining large grained crystals of uniform composition; this was eventually attributed to an inability to control the temperature profile in the high pressure furnace during recrystallization. The technique finally adopted involved compounding and rapid solidification in the high pressure furnace followed by recrystallization of segments of the ingot in sealed quartz ampoules in a conventional furnace with a flat temperature profile. ** were encountered*

In the earlier stages of the work, some measurements were made to try to define the liquidus and solidus curves of the pseudo-binary phase diagram of mercury-telluride and cadmium-telluride. Though the high pressure furnace permits precise measurement of temperature, commensurate precision in the corresponding melt composition is not possible. During liquidus determinations the quantity of mercury in reflux is unknown and due to poor mixing the melt is mercury rich at the surface and off the desired stoichiometry in the bulk. Until the final stages of the program we were unable to prepare significantly sized crystals of uniform composition. The earlier attempts to measure solidus temperatures could not be related to composition. Polycrystalline ingots of apparent uniform composition by density measurements undergo phase segregation during solidification so that the first temperature transition observed on melting is that of the mercury telluride eutectic that melts at 680°C. No other transitions are clearly defined. Despite these reservations the data are presented in detail since the basic information is open to other interpretation.

UNCLASSIFIED

SECURITY CLASSIFICATION OF THIS PAGE(When Data Entered)

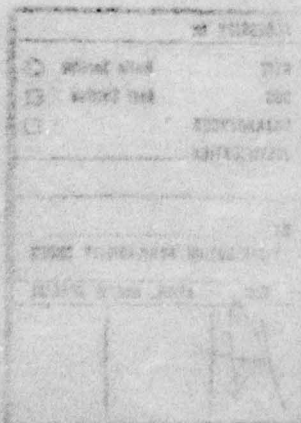
FOREWORD

This Final Technical Report describes work supported by the Air Force Materials Laboratory from June 1, 1973 through April 1, 1976, at Arthur D. Little, Inc., Detection Sciences Group, 15 Acorn Park, Cambridge, Massachusetts 02140, under Contract No. F33615-73-C-5155, monitored by Mr. R. L. Hickmott, AFML/LPO, under Project No. FY1457-73-00342/7371. The principal investigator was initially Dr. J. M. Steininger, assisted by Dr. J. F. Butler. The work was completed by Dr. John M. Parry. Initial funding was provided by the Air Force Materials Laboratory Director's Funds.

ACCESSION NO.	
DTIC	DTIC Status <input checked="" type="checkbox"/>
DDC	DDC Status <input type="checkbox"/>
UNANNOUNCED	<input type="checkbox"/>
JUSTIFICATION.....	
BY.....	
DISTRIBUTION / AVAILABILITY CODES	
Dist.	ANAL. and/or SPECIAL
AH	

TABLE OF CONTENTS

<u>SECTION</u>		<u>Page</u>
I	INTRODUCTION	1
II	PHYSICAL AND THERMODYNAMIC PROPERTIES	4
	A. INTRODUCTION	4
	B. VAPOR PRESSURE	6
	C. ALLOY SEGREGATION	8
	D. HIGH PRESSURE FURNACE TECHNIQUE	10
III	EXPERIMENTAL APPROACH	12
	A. CRYSTAL GROWTH AND ANNEALING	12
	B. MATERIALS CHARACTERIZATION	12
	C. DETECTOR FABRICATION AND TESTING	15
	D. PHASE DIAGRAM DETERMINATION	21
	E. EVALUATION OF RESULTS	27
IV	MATERIALS PREPARATION	33
V	DISCUSSION	49
VI	REFERENCES	50



LIST OF ILLUSTRATIONS

<u>FIGURE</u>		<u>Page</u>
1	Spectral Detectivity of HgCdTe Detectors Fabricated From High Pressure Furnace Material	2
2	Physical and Thermodynamic Properties of HgTe-CdTe Alloys	5
3	Schematic Pressure-Temperature Phase Diagram For $\text{Hg}_{1-x}\text{Cd}_x\text{Te}$ Alloy System	7
4	Theoretical Solidification Profiles For $\text{Hg}_{.50}\text{Cd}_{.50}\text{Te}$ Alloy	9
5	ADL Model HP High Pressure Furnace-Detection Sciences Group Unit	13
6	$\text{Hg}_{.80}\text{Cd}_{.20}\text{Te}$ Ingot Grown in High Pressure Furnace	14
7	$\text{Hg}_{.80}\text{Cd}_{.20}\text{Te}$ Crystal Wafers	16
8	Longitudinal Composition Profile of HgCdTe Ingot (Density Measurements)	17
9	Radial Composition Profiles of HgCdTe Wafers (Microprobe Analysis)	18
10	Circuit and Geometry of Photoconductive Detectors	19
11	HgCdTe Photoconductive Detectors	20
12	HgCdTe ₂₂ -Element Detector Array	22
13	Hg-Cd-Te Pressure-Temperature Phase Diagram	29
14	Pseudobinary HgTe-CdTe Phase Diagram	30
15	Method of Slicing Ingot 47	34

LIST OF TABLES

<u>TABLE</u>		<u>Page</u>
I	Performance Data of 15-Element HgCdTe Detector Array	23
II	Pressure-Temperature Data for Hg Vapor	25
III	Pressure-Temperature Data for the Hg-Te System	26
IV	Pressure-Temperature Data for the Hg _{.70} Cd _{.30} -Te System	28
V	Densities and X Values for Vertical Slices of Preparation 47	35
VI	Densities and X Values for Sections B and C of Preparation 47	36
VII	Density Values for Crystal 55	39
VIII	Density Values for Crystal 56	40
IX	Bar Densities for Slices 20, 21, 42 and 43 for Crystal 57	42
X	Densities and X Values for Crystal 61	44
XI	Orthogonal Bar Densities of Slices 10 and 11 for Crystal 61	45
XII	Orthogonal Bar Densities of Slices 9 and 10 for Crystal 61	46

SECTION I

INTRODUCTION

The objective of this program was to develop the application of high pressure furnace technology to the preparation of the ternary alloy mercury cadmium telluride $\text{Hg}_{1-x}\text{Cd}_x\text{Te}$. This material is of interest to the Air Force for the fabrication of detector arrays operating in the infrared spectrum.

For x values higher than 0.15, $\text{Hg}_{1-x}\text{Cd}_x\text{Te}$ is an intrinsic semiconductor which can be used for the fabrication of high performance infrared detectors operating at relatively elevated temperatures. Because of the continuous variation of the energy bandgap with composition x , HgCdTe detectors can be designed to achieve peak performance at wavelengths varying from about 1 μm to above 14 μm . This includes the important spectral regions of 8 to 14 μm , 3 to 5 μm and near 2 μm . Crystal growth and annealing techniques were initially developed for material with x near 0.20 and this is now the semiconductor of choice for infrared detectors operating in the 8 to 14 μm region at 77°K. In other regions of the spectrum, the technology of HgCdTe detectors is less well developed, primarily because of the increased difficulties of material preparation. Theoretical investigations and experimental devices, however, show that $\text{Hg}_{1-x}\text{Cd}_x\text{Te}$ is also capable of high performance in the near and middle infrared regions. Figure 1 shows the spectral detectivity of single element photoconductive and photovoltaic detectors fabricated at ADL from high pressure furnace grown material. The peak wavelengths for these detectors vary from 2.7 to 11 μm .

Even for 8 to 14 μm material, however, the development of a technology for the preparation and growth of uniform large crystals of $\text{Hg}_{1-x}\text{Cd}_x\text{Te}$ suitable for large-scale detector fabrication has long been handicapped by two main difficulties: the high mercury vapor pressure over molten material which makes preparation techniques hazardous and poorly reproducible and the extensive segregation of the alloy upon solidification

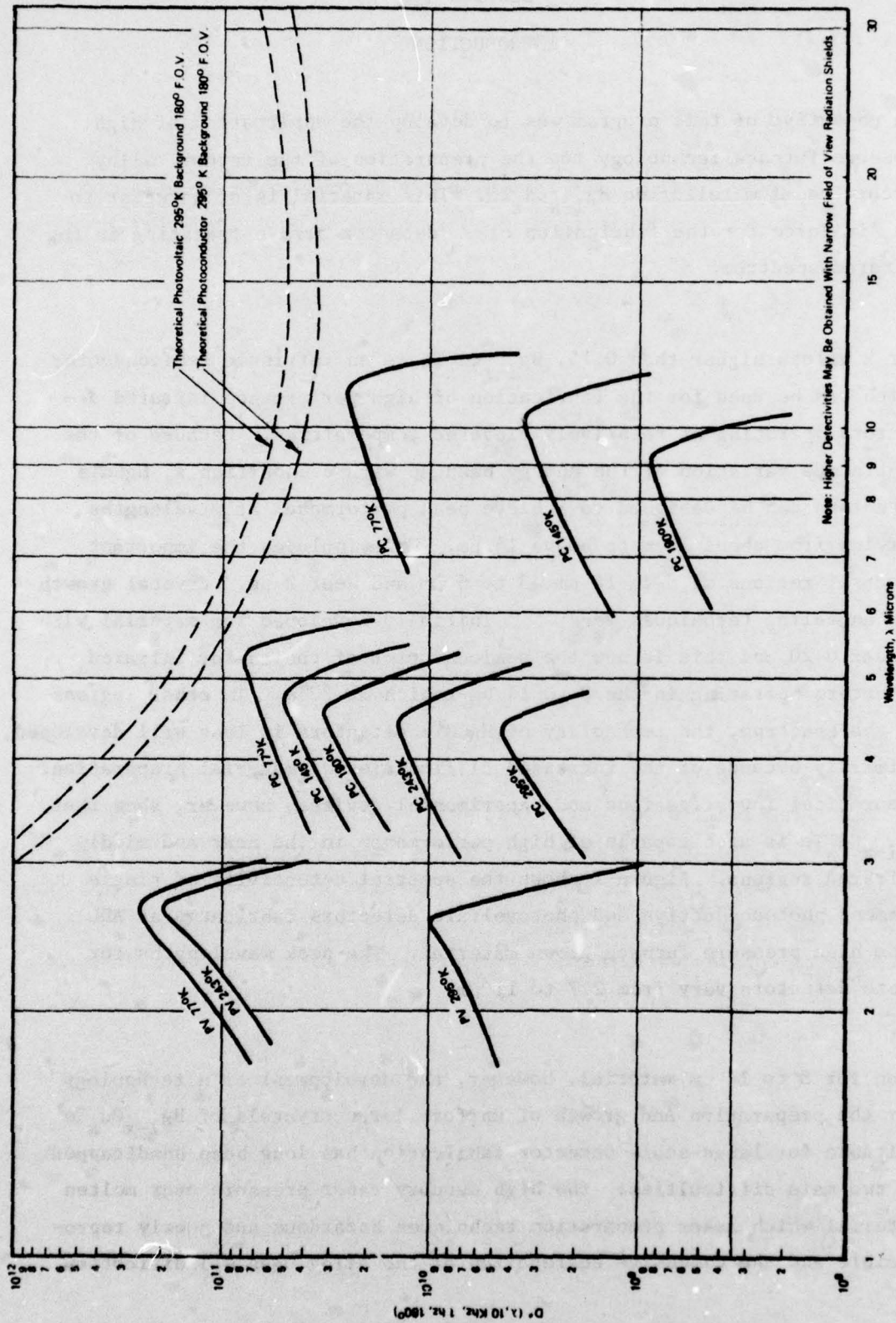


FIGURE 1 SPECTRAL DETECTIVITY OF HgCdTe DETECTORS FABRICATED FROM HIGH PRESSURE FURNACE MATERIAL

which results in poor control of compositional uniformity. Because of the increase in melt temperature, the problem of high vapor pressure becomes even more severe for middle and short wavelength material.

Because of the deviations from stoichiometry at high temperatures, $\text{Hg}_{1-x}\text{Cd}_x\text{Te}$ grown from the melt under equilibrium or near equilibrium conditions is tellurium-rich and yields p-type material. Since the fabrication of high performance photoconductive detectors requires low carrier concentration n-type material, melt grown $\text{Hg}_{1-x}\text{Cd}_x\text{Te}$ has to be annealed at low temperature in Hg vapor to achieve type conversion. For short wavelength material, conventional annealing techniques require low temperatures where the diffusion rates are low. It was another main objective of this program to investigate annealing at high temperatures and high mercury vapor pressures to increase the rate of type conversion for short wavelength material.

One of the advantages of the high pressure furnace technique developed at ADL consists of the use of open crucibles where the pressure of the inert gas inside the high pressure furnace balances the vapor pressure of the volatile materials over the charge. This allows the direct introduction of thermocouples into the melt for temperature profiling and for thermal analysis under controlled vapor pressure. In this program, the liquidus curve was examined by thermal analysis of cooling curves for various compositions in the 0.30 - 0.40 range as a function of pressure. Attempts were also made to determine selected points on the solidus curve. This data is coupled with thermodynamic calculations of the liquidus-solidus equilibrium to establish the pseudobinary phase diagram in this range of compositions.

SECTION II

PHYSICAL AND THERMODYNAMIC PROPERTIES

A. INTRODUCTION

Figure 2 shows the variation with composition of the fundamental physical and thermodynamic properties of $\text{Hg}_{1-x}\text{Cd}_x\text{Te}$ pseudobinary alloys:

- energy bandgap at 77 K,
- corresponding cut-off wavelength,
- liquidus and solidus temperatures (pseudobinary T-x phase diagram), and
- vapor pressure at 25-30°C above the liquidus temperature.

The bandgap varies approximately linearly⁽²⁾ from 1.6 eV for the wide bandgap semiconductor CdTe to -0.3 eV for the semimetal HgTe. The crossover composition (zero bandgap) is for an x value of approximately 0.15. Above this value $\text{Hg}_{1-x}\text{Cd}_x\text{Te}$ is an intrinsic semiconductor. The corresponding cut-off wavelength of photoresponse therefore varies from about 1 to 14 μm and beyond.

The liquidus temperatures shown in Figure 2 were estimated

at ADL by thermal analysis of cooling curves in a high pressure furnace and are in good agreement with the earlier data of Blair and Newnham⁽³⁾ The solidus temperatures have been calculated⁽⁴⁾ from the liquidus data and from the heats of fusion of the end compounds by application of the ideal liquidus-solidus thermodynamic equilibrium equation.

The vapor pressure values shown in Figure 2 represent data

also obtained in the high pressure furnace. They show a rapid increase with x value despite the decrease in Hg concentration in the

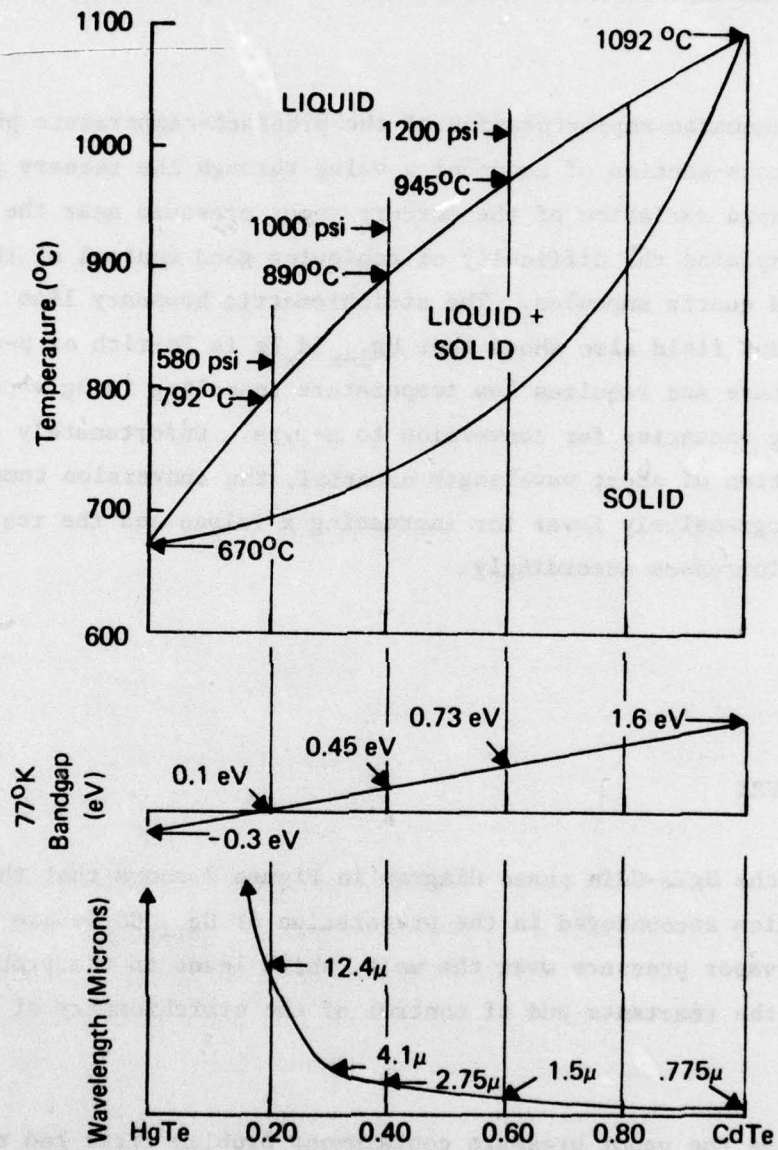


FIGURE 2 PHYSICAL AND THERMODYNAMIC PROPERTIES OF HgTe-CdTe ALLOYS

melt. For $x = 0.40$, the pressure reaches 66 atmospheres (1000 psi), which is significantly above the safety limit for heavy wall quartz ampoules.

Figure 3 is a schematic representation of the pressure-temperature phase diagram for a cross-section of constant x value through the ternary phase diagram. The rapid variation of the mercury vapor pressure near the melting point explains the difficulty of achieving good control of the system in sealed quartz ampoules. The stoichiometric boundary line inside the solidus field also shows that $\text{Hg}_{1-x}\text{Cd}_x\text{Te}$ is Te-rich or p-type at high temperature and requires low temperature annealing in Hg vapor to reduce the Hg vacancies for conversion to n-type. Unfortunately for the preparation of short wavelength material, the conversion temperature becomes progressively lower for increasing x values and the required annealing time increases accordingly.

B. VAPOR PRESSURE

Examination of the HgTe-CdTe phase diagram in Figure 2 shows that the major difficulties encountered in the preparation of $\text{Hg}_{1-x}\text{Cd}_x\text{Te}$ are related to the high Hg vapor pressure over the melt, which leads to the problems of containment of the reactants and of control of the stoichiometry of the material.

Attempts to solve the vapor pressure containment problem first led to the development of sealed quartz ampoule techniques. These techniques rely on the use of small diameter (usually 10 millimeters I.D.), heavy wall, sealed quartz ampoules to contain the pressure of Hg, and on slow heating in specially designed furnaces to prevent explosions. With pressures already of the order of 35 to 40 atmospheres for 8 to 14 μm material, the risk and frequency of explosions increase rapidly for the middle

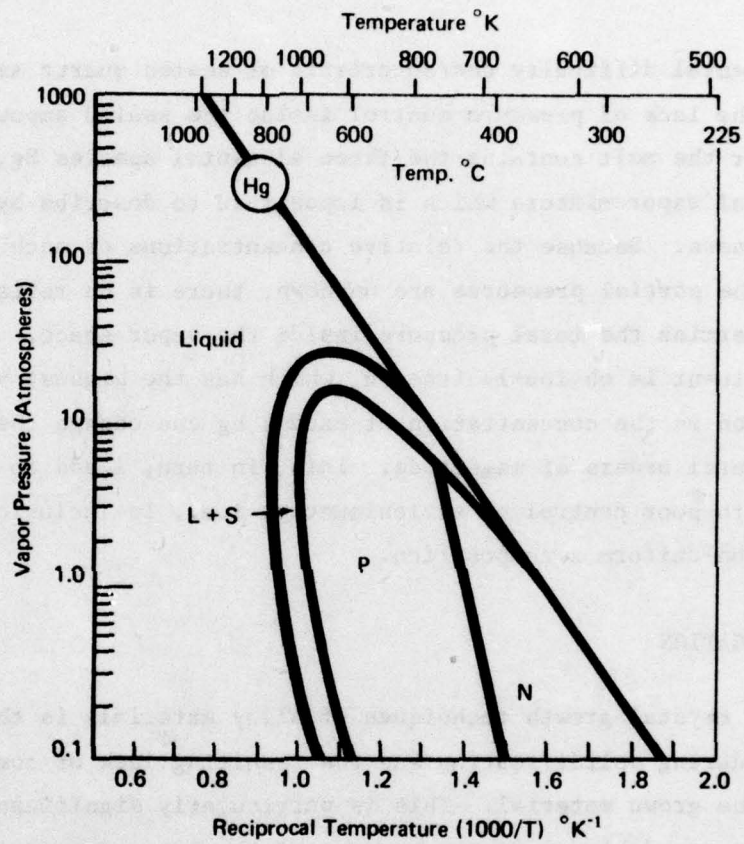


FIGURE 3 SCHEMATIC PRESSURE-TEMPERATURE PHASE DIAGRAM FOR $Hg_{1-x}Cd_xTe$ ALLOY SYSTEM

and short wavelength materials. As a rule, therefore, conventional sealed quartz ampoule techniques are restricted to compositions around 0.20 (8 to 14 μm material) and to diameters of about 10 millimeters.

A second fundamental difficulty characteristic of sealed quartz ampoule techniques is the lack of pressure control inside the sealed ampoule. The vapor space over the melt contains the three elemental species Hg, Cd and Te in a non-ideal vapor mixture which is impossible to describe by the simple laws of ideal gases. Because the relative concentrations of each vapor species and therefore the partial pressures are unknown, there is no reliable or precise way to determine the total pressure inside the vapor space. The most critical constituent is obviously free Hg, which has the highest vapor pressure. A small variation in the concentration of excess Hg can change the internal pressure by several orders of magnitude. This, in turn, leads to low reproducibility due to poor control of stoichiometry, i.e., Te inclusions or Hg blowholes and non-uniform x composition.

C. ALLOY SEGREGATION

Inherent in all crystal growth techniques of alloy materials is the problem of segregation during solidification and the resulting lack of compositional uniformity in the grown material. This is particularly significant in the case of the HgTe-CdTe pseudobinary system because of the large separation between the liquidus and solidus curves (Figure 2) which indicates high values of the segregation coefficient. The theoretical solidification profiles of Figure 4 show the composition of the solid phase (abscissa) as a function of the composition ratio or segregation coefficient. The lowest curve demonstrates that slow cooling of a charge of molten $\text{Hg}_{1-x}\text{Cd}_x\text{Te}$ is characterized by initial solidification of CdTe-rich material which leads to an enrichment of the melt in HgTe and to solidification of material becoming progressively richer in HgTe. In other words, short wavelength material freezes out first and is followed by material of progressively longer wavelength. This compositional variation is advantageous for preliminary research programs in the sense that a few crystals can yield a selection of small regions with high x values. It

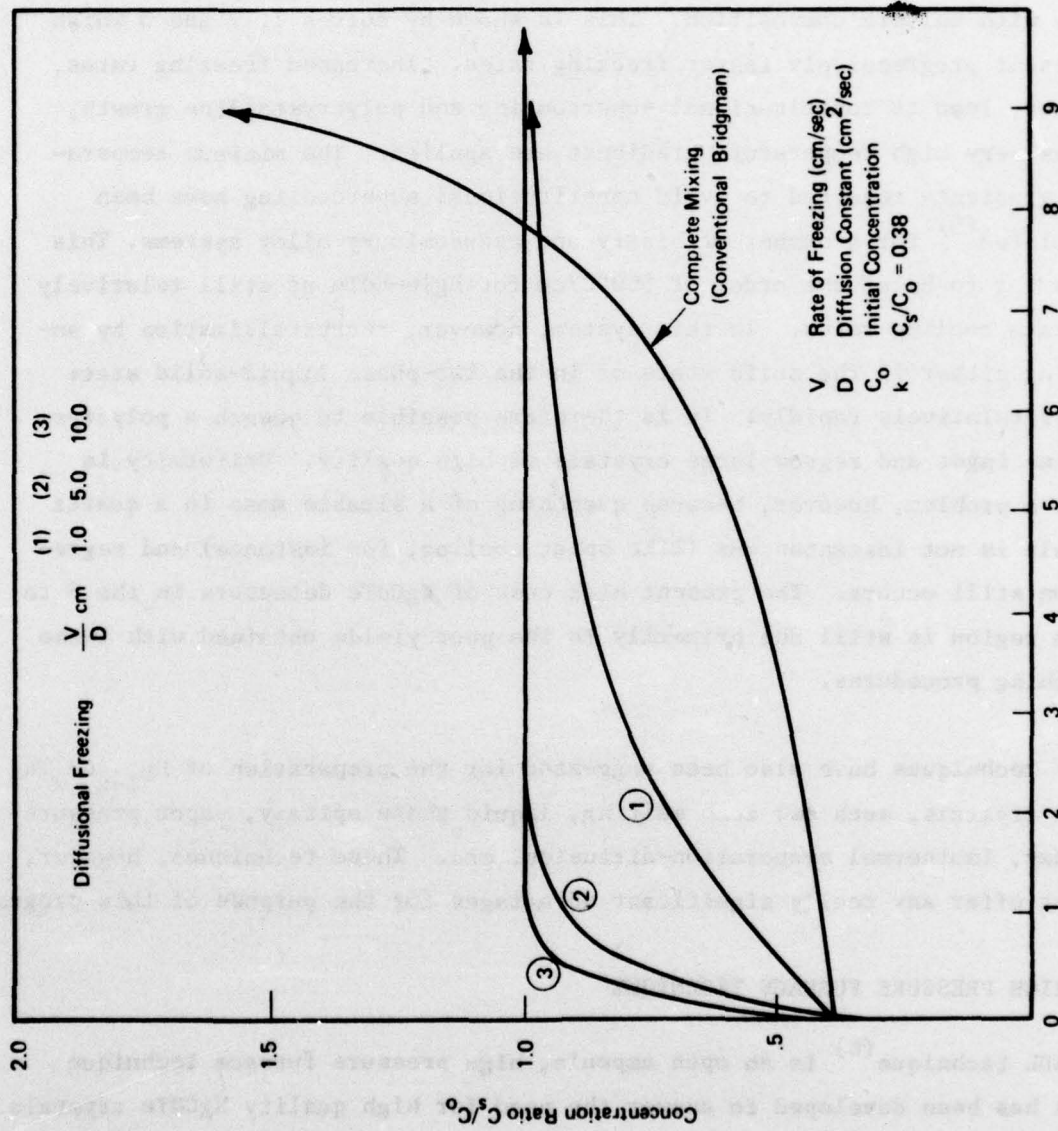


FIGURE 4 THEORETICAL SOLIDIFICATION PROFILES FOR Hg₅₀Cd₅₀Te ALLOY

is, however, inadequate for large-scale production of uniform material of controlled composition.

An apparently simple solution consists in fast quenching of the molten alloy in an attempt to prevent diffusion and obtain a freeze-in of an alloy with uniform composition. This is shown by curves 1, 2 and 3 which represent progressively faster freezing rates. Increased freezing rates, however, lead to constitutional supercooling and polycrystalline growth, unless very high temperature gradients are applied. The minimum temperature gradients required to avoid constitutional supercooling have been calculated⁽⁵⁾ for a number of binary and pseudobinary alloy systems. This turns out to be of the order of 500°C/cm for HgTe-CdTe at still relatively moderate cooling rates. In this system, however, recrystallization by annealing either in the solid state or in the two-phase liquid-solid state occurs relatively rapidly. It is therefore possible to quench a polycrystalline ingot and regrow large crystals of high quality. Uniformity is still a problem, however, because quenching of a sizable mass in a quartz ampoule is not instantaneous (like splat cooling, for instance) and segregation still occurs. The present high cost of HgCdTe detectors in the 8 to 14 μm region is still due primarily to the poor yields obtained with these quenching procedures.

Other techniques have also been suggested for the preparation of $\text{Hg}_{1-x}\text{Cd}_x\text{Te}$ alloy crystals, such as: zone melting, liquid phase epitaxy, vapor pressure epitaxy, isothermal evaporation-diffusion, etc. These techniques, however, do not offer any really significant advantages for the purpose of this program.

D. HIGH PRESSURE FURNACE TECHNIQUE

The ADL technique⁽⁶⁾ is an open ampoule, high pressure furnace technique which has been developed to answer the need for high quality HgCdTe crystals suitable for large-scale fabrication of IR devices, i.e., large numbers of discrete elements or arrays, and large area devices.

This technique is characterized by:

- improved safety and reliability, the use of open ampoules in a high pressure inert gas atmosphere practically eliminates explosions and ampoule failures;
- improved pressure control by the development of a pressure balancing technique whereby the pressure of inert gas inside the furnace is utilized to control the Hg vapor pressure over the charge;
- increased ingot diameter since the open quartz ampoule is not under stress; standard size is 1-inch diameter and could be further increased if required;
- increased range of compositions available due to the high pressure capability (100 atmospheres) of the furnace, which covers the requirements for HgCdTe alloys up to and above $x = 0.60$ (1 μm material and less);
- improved materials quality by the combination of all of the above factors and evidenced by the high performance of photoconductive and photovoltaic detectors made from this material.

SECTION III

EXPERIMENTAL APPROACH

A. CRYSTAL GROWTH AND ANNEALING

The high pressure furnace of the Detection Sciences Group (Figure 5) is a resistance-heated ADL model HP furnace designed to operate at up to 100 atmospheres of inert gas pressure. The water-cooled stainless steel pressure chamber is equipped with two pulling heads for synchronized or independent rotation and vertical translation of the crucible stage and upper monitoring thermocouple. Two water-cooled windows allow for direct viewing or remote TV control of the interior of the chamber. Solid metal liners or liquid-metal heat pipes⁽⁷⁾ can be placed inside the graphite heater assembly to obtain more uniform temperature profiles under high pressure.

In a typical crystal growth run, the HgCdTe charge containing a stoichiometric mixture of the high purity elements plus a small excess of Hg for vapor pressure control is loaded under inert gas atmosphere into a high purity, etched and cleaned quartz ampoule. Prior to loading, the commercial high purity double-zone refined cadmium and tellurium are further purified in our laboratory by multiple zone refining under a flow of palladium-diffused high purity hydrogen. The crystal growth ampoule containing the charge is then placed inside the high pressure furnace which is flushed several times and pressurized with high purity argon to 100 atmospheres. The charge is rapidly heated to 25-30°C above the liquidus temperature, homogenized for 10 to 20 minutes, solidified by programmed cooling under controlled pressure and recrystallized by high temperature annealing for periods varying from several days to several weeks. If required, type conversion is achieved by low temperature annealing under reduced Hg vapor pressure.

B. MATERIALS CHARACTERIZATION

The standard ingot size now produced in the high pressure furnace (Figure 6) has a 1-inch diameter and a length of 2 to 3 inches. The weight of about

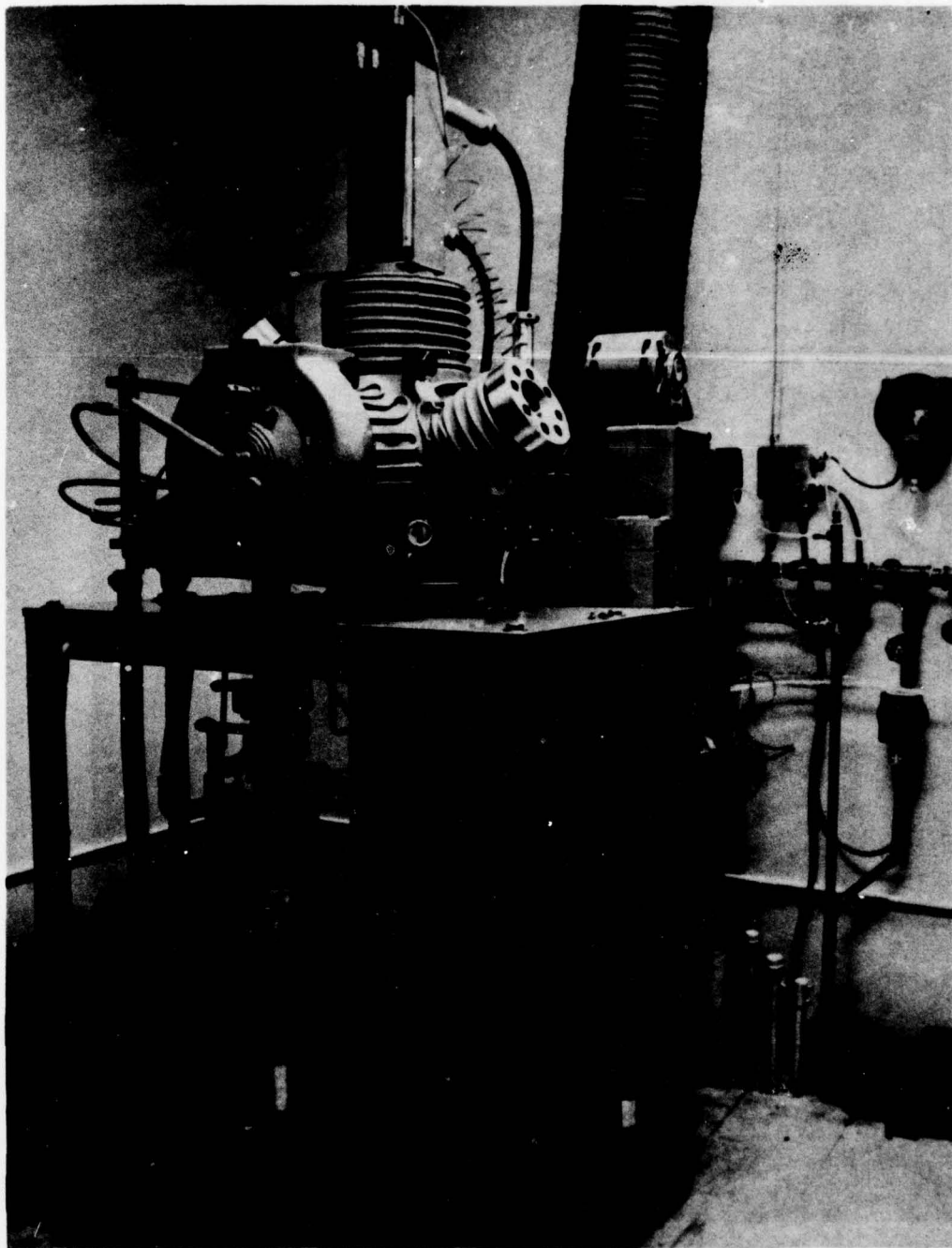


**FIGURE 5 ADL MODEL HP HIGH PRESSURE FURNACE –
DETECTION SCIENCES GROUP UNIT**

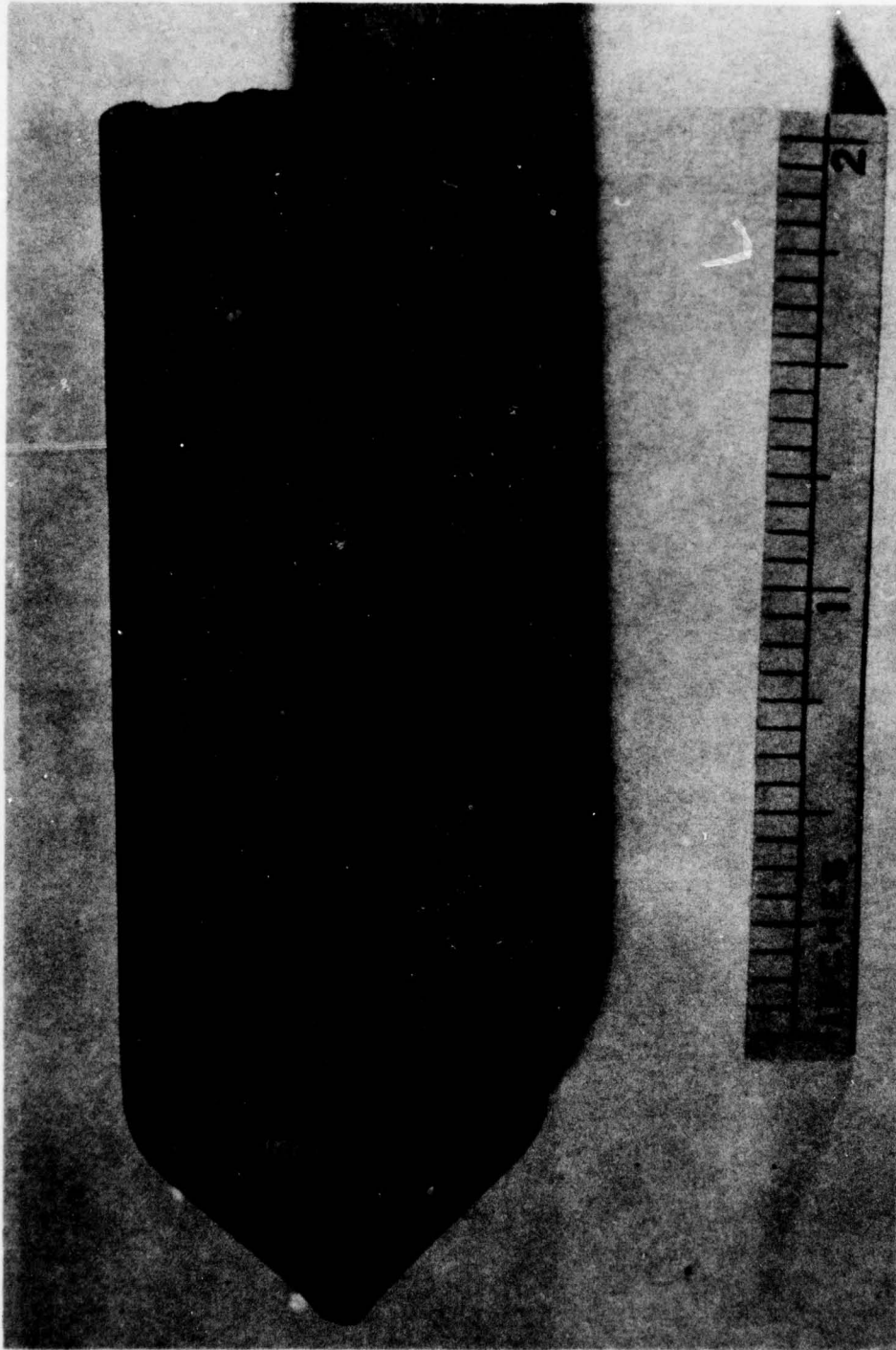


FIGURE 6 $\text{Hg}_{.80}\text{Cd}_{.20}\text{Te}$ INGOT GROWN IN HIGH PRESSURE FURNACE

200 grams varies slightly with composition. The crystal grain boundaries on the surface of the ingot shown in Figure 6 are made apparent by a light sandblasting with alumina powder.

The ingots are normally sliced along their length into 1-inch diameter wafers by cutting with a fine wire saw. The internal crystal structure is then readily apparent (Figure 7). Individual crystal sizes vary with annealing conditions up to a full inch in diameter.

Longitudinal composition profiles of the ingots are obtained by determining the density of the 1-mm thick wafers cut along the length of the ingot. For example, the profile shown in Figure 8 shows a uniform composition along an ingot averaging $x = 0.212 \pm 0.008$ which corresponds to the experimental errors of measurement. It should be noted, however, that this data was derived from a polycrystalline ingot obtained by rapid solidification.

Radial composition profiles are determined by electron microprobe analysis using scanning and step counting techniques. The electron microprobe data in Figure 9 shows the average of six counts for the Cd L_{α} X-ray line taken with a beam spot of 50-micron diameter at 0.1-inch increments along the diameter of the 1-inch wafer. The average variation of 0.212 ± 0.007 is also of the order of magnitude of the experimental errors.

C. DETECTOR FABRICATION AND TESTING

HgCdTe photoconductive detectors were made from n-type material with electron concentrations in the range of 10^{15} to 10^{14} cm^{-3} . The geometry of a photoconductive detector is shown in Figure 10. It consists of a thin parallelepiped of semiconductor crystal epoxied to an insulating substrate. Each detector element (Figure 11) is delineated by photolithographic techniques similar to those used for fabrication of mesa transistors. The active area of the detector is defined by evaporating metal contact layers on the upper surface. Leads are attached by thermocompression or ultrasonic bonding. For low temperature operation, the detector is mounted in an evacuated package, such as a metal or glass dewar or a cold-finger pack.

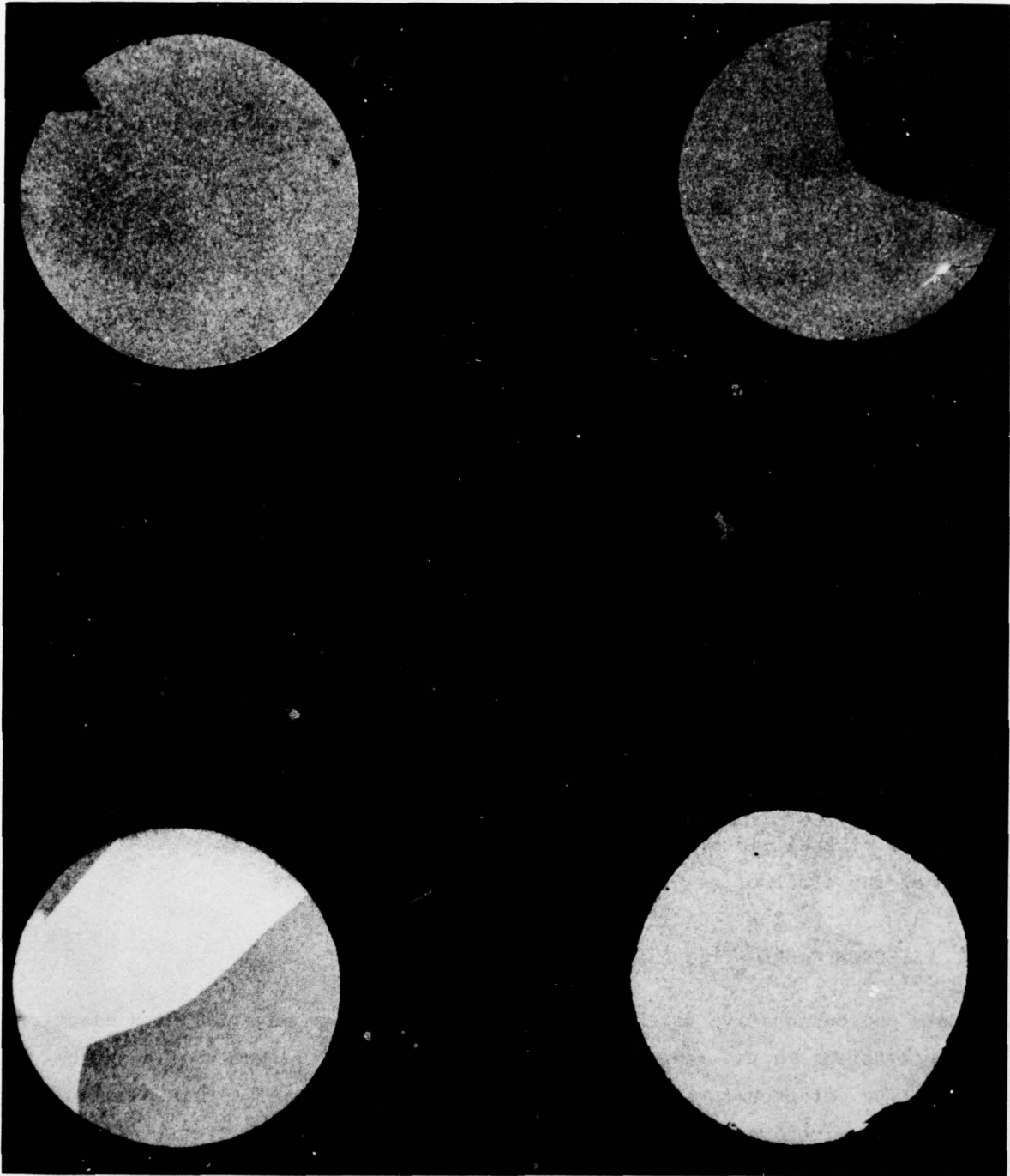
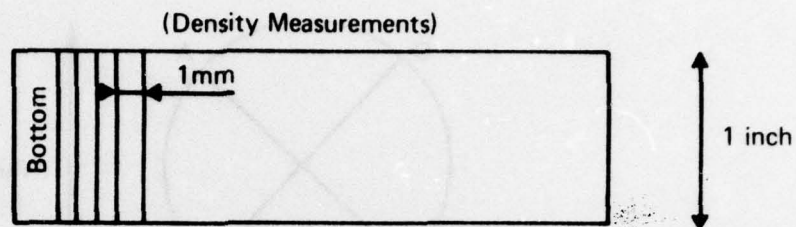


FIGURE 7 Hg₈₀Cd₂₀Te CRYSTAL WAFERS

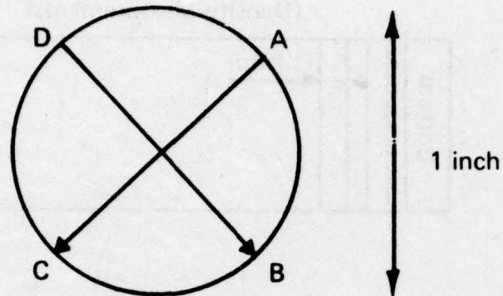


Slice	Density	Composition	Slice	Density	Composition
Bottom	7.626	0.202	25	7.645	0.194
8	7.633	0.199	26	7.594	0.216
9	7.631	0.200	27	7.575	0.219
10	7.628	0.201	28	7.581	0.222
11	7.632	0.199	29	7.595	0.216
12	7.622	0.204	30	7.584	0.221
13	7.620	0.205	31	7.591	0.218
14	7.607	0.211	32	7.586	0.220
15	7.604	0.212	33	7.578	0.224
16	7.600	0.214	34	7.572	0.226
17	7.596	0.215	35	7.595	0.216
18	7.605	0.212	36	7.570	0.227
19	7.609	0.210	37	7.585	0.221
20	7.565	0.229	38	7.582	0.221
21	7.603	0.213	39	7.597	0.215
22	7.614	0.207	40	7.604	0.212
23	7.635	0.198	41	7.601	0.213
24	7.627	0.202	42	7.603	0.212

Mean: 0.212

Standard Derivation: 0.008

FIGURE 8 LONGITUDINAL COMPOSITION PROFILE OF HgCdTe INGOT
(Density Measurements)

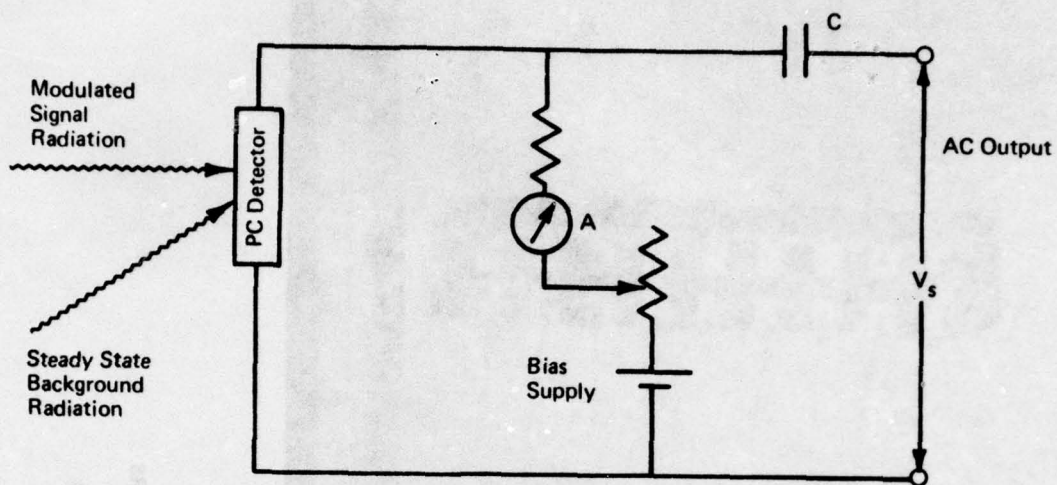


AC Diameter			BD Diameter		
Step	Counts	Composition	Step	Counts	Composition
1	65	.214	1	69	.221
2	67	.220	2	66	.212
3	63	.207	3	63	.202
4	64	.211	4	65	.208
5	63	.207	5	63	.202
6	67	.220	6	67	.215
7	61	.201	7	65	.208
8	69	.227	8	67	.215
9	61	.207	9	70	.224
Mean	64.4	.212	Mean	66.1	.212

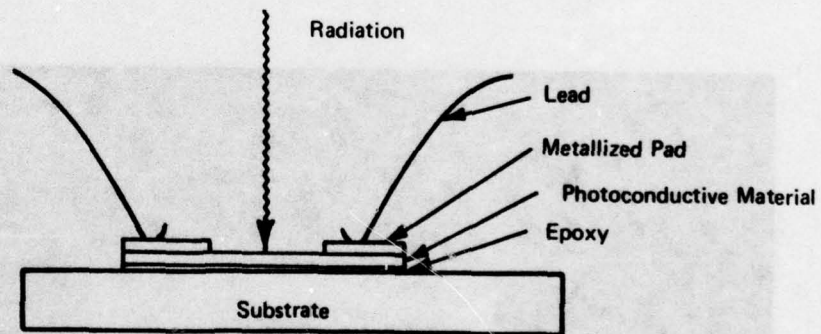
Mean: 0.212

Standard Deviation: 0.007

FIGURE 9 RADIAL COMPOSITION PROFILES OF HgCdTe WAFERS (Microprobe Analysis)



a. Schematic Circuit of Photoconductive Detector



b. Geometry of Photoconductive Detector

FIGURE 10 CIRCUIT AND GEOMETRY OF PHOTOCONDUCTIVE DETECTORS

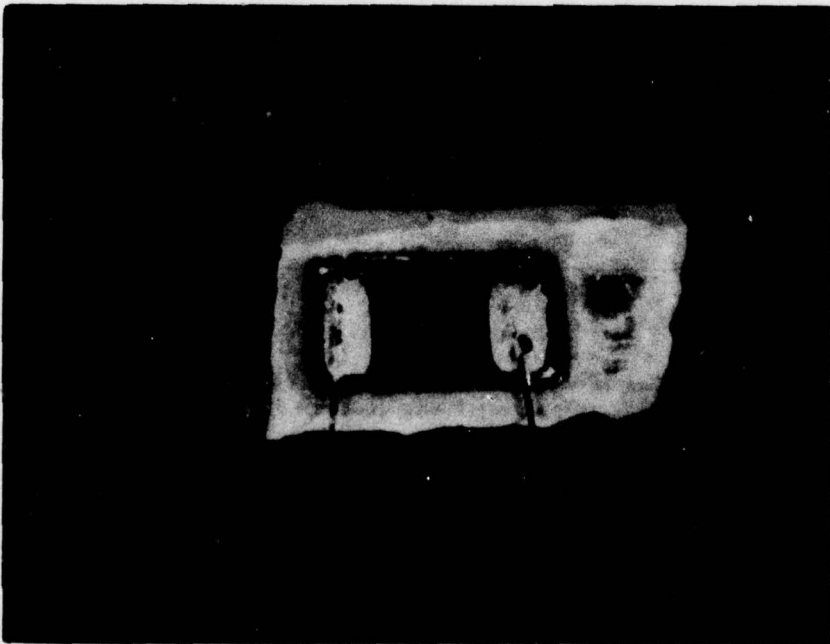
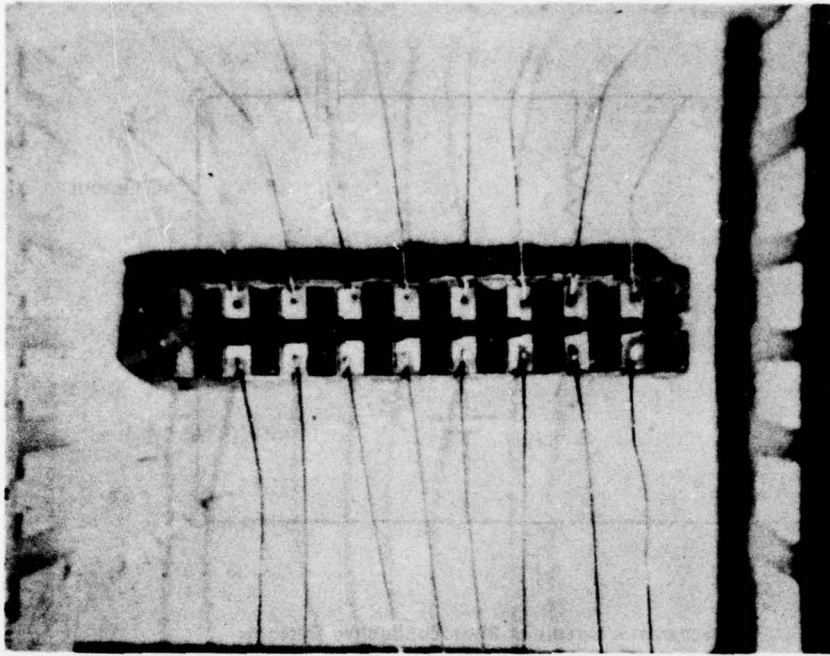


FIGURE 11 HgCdTe PHOTCONDUCTIVE DETECTORS
A. 0.5mm x 0.5mm Active Area
B. 25 μ x 25 μ to 200 μ x 200 μ Active Areas

Critical steps in the fabrication of photoconductive detectors include the lapping, polishing and etching of the thin (10 to 15 microns) crystal wafer to close tolerances without introducing substantial damage in the material. ADL has developed an integrated technology for the fabrication of single element detectors and high density arrays. Single element detector sizes fabricated to date range from $2.5 \times 2.5 \text{ mm}^2$ (.100" x .100") to $25\mu \times 25\mu$ (.001" x .001"). Linear arrays with .002" separation between elements are also being fabricated (Figure 12).

The finished detectors are tested on a blackbody test station for response and detectivity. A spectral responsivity curve is determined with a double beam spectrometer. A spot scanner is used for evaluating the spatial uniformity. The high frequency response of the signal is measured with an ADL Lead-salt laser test set (Model LITS).

The high performance and high uniformity measured on various arrays (Table I) attest to the high quality of the material.

D. PHASE DIAGRAM DETERMINATION

Figures 2 and 3 show that because of the presence of Hg, the phase diagram of the Hg-Cd-Te system is highly dependent on vapor pressure. The optimization of crystal growth and annealing techniques therefore requires extensive phase diagram information.

One of the advantages of the ADL high pressure furnace technique is due to the use of open crucibles where the pressure of inert gas inside the high pressure chamber balances the vapor pressure of the volatile materials over the charge. This technique makes it possible to introduce thermocouples inside the melt for temperature profiling and thermal analysis under controlled vapor pressure.

The preliminary vapor pressure and liquidus temperature data shown in Figure 2 for the pseudobinary HgTe-CdTe system were obtained in this way by slow cooling of homogenized melts under constant pressure. By varying

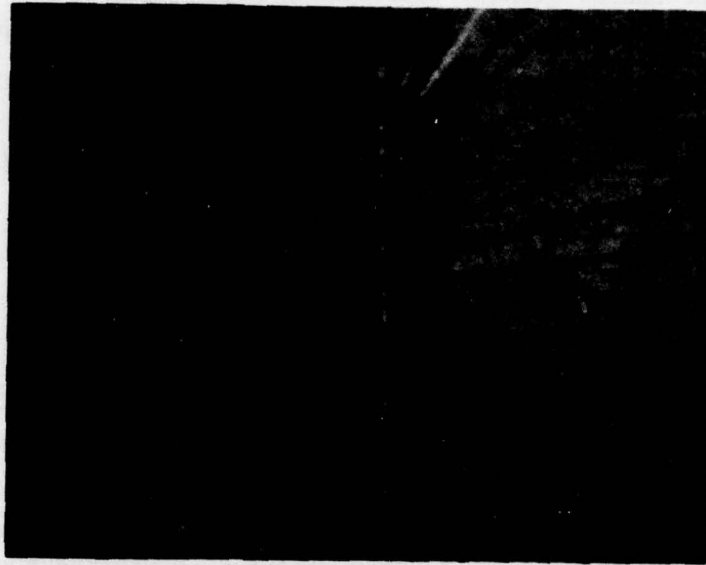


FIGURE 12 HgCdTe 22 - ELEMENT DETECTOR ARRAY

TABLE I

Performance Data of 15-Element HgCdTe Detector Array

CONFIGURATION: Straight Linear Array
 ACTIVE AREA: .002 in. x .0024 in.
 SPACING BETWEEN ELEMENTS: .002 in.
 WINDOW: IRtran-2
 FIELD OF VIEW: 180°
 PEAK WAVELENGTH: 11 ±1 Micrometers

TEST CONDITIONS: Constant Applied Field:
 120 mV (24 V/cm)

Number	Resistance 77 K (ohms)	Bias (mA)	$R_{\lambda\rho}$ (V/W)	$D^*_{\lambda\rho}$ cm-Hz ^{1/2} /W
1	28.6	4.2	19,600	2.7×10^{10}
2	21.5	5.6	15,200	2.9×10^{10}
3	27.6	4.35	12,800	2.1×10^{10}
4	40.2	3.0	17,400	1.7×10^{10}
5	26.0	4.6	11,000	1.9×10^{10}
6	25.0	4.8	22,000	2.0×10^{10}
7	14.0	8.5	8,600	2.7×10^{10}
8	34.2	3.5	6,100	1.5×10^{10}
9	24.5	4.9	18,800	1.8×10^{10}
10	18.0	6.7	11,900	1.8×10^{10}
11	13.2	9.1	6,600	2.0×10^{10}
12	19.35	6.2	21,100	2.2×10^{10}
13	16.5	7.3	18,500	2.5×10^{10}
14	23.5	5.1	12,800	1.8×10^{10}
15	16.2	7.4	10,800	1.9×10^{10}
Average	<u>23.2</u>		<u>14,200</u>	<u>2.1×10^{10}</u>

the pressure of the inert gas, pressure-temperature cross-sections of the phase diagrams can also be determined. The determination of solidus temperatures is done by slow heating under constant pressure.

The determination of the pressure-temperature phase diagrams of the ternary Hg-Cd-Te system in this program is based on a dual method which combines thermal analysis of cooling curves and determination of pressure-temperature curves over the melt, i.e., above and near the liquidus temperature. This dual determination technique improves the degree of accuracy and reliability for both liquidus temperature and pressure. For the solidus curve, however, only the temperature is determined experimentally because of the complications due to segregation.

The procedure is the following. A charge of desired composition is loaded into a quartz ampoule, placed in the high pressure furnace, reacted and melted under high inert gas pressure. The pressure-temperature (P-T) curve over the melt is first determined by equilibrating the charge at given pressures of inert gas and by recording the temperature of a chromel-alumel thermocouple inserted inside the melt within a close-fitting quartz protection tube. This normally yields a series of points which approximate a straight line on a plot of $\ln P$ vs. $1/T$. When the temperature is brought progressively lower, a break is eventually observed in the curve which corresponds to the onset of freezing, i.e., to the liquidus. For thermal analysis, the charge is remelted under a slight excess of inert gas pressure. The furnace power is turned off and a cooling curve under constant pressure is recorded as a function of time. The liquidus arrest temperature is obtained from the break in the classical temperature-time cooling curve.

The solidus temperature is obtained by a similar technique by heating the solid charge after homogenization by annealing for about 15 hours. This technique has been successively applied to the determination of the vapor pressure curve of pure Hg (Table II), the liquidus-solidus equilibrium of the binary Hg-Te system (Table III) and the liquidus and solidus of the

TABLE II

Pressure-Temperature Data
for Hg Vapor

Pressure		Temperature		ln P	$\frac{10^3}{T}$
psi	atm	°C	K		
1440	98.0	798	1071	4.585	0.934
1250	85.0	776	1049	4.443	0.953
1206	82.0	765	1038	4.407	0.964
1000	68.0	741	1014	4.220	0.986
850	57.8	713	986	4.057	1.015
611	45.0	683	956	3.806	1.047
510	34.7	648	921	3.547	1.086
380	25.9	622	895	3.252	1.118
300	20.4	590	863	3.159	1.159
221	15.0	563	836	2.710	1.196
170	11.6	536	809	2.448	1.236
132	9.0	516	789	2.195	1.267

TABLE III

Pressure-Temperature Data
for the Hg-Te System

Composition	Pressure		Temperature		$\frac{10^3}{T}$	Effect
	psi	atm	°C	K		
Hg _{.50} Te _{.50}	450	30.6	770	1043	0.959	Melt P-T
	308	20.95	729	1002	0.998	"
	250	17.0	684	957	1.045	"
	225	15.3	671	944	1.06	"
	400	27.2	665	938	1.066	Liquidus Arrest
	337	27.9	6666	939	1.065	"
	300	20.4	669	942	1.062	"
	300	20.4	668	941	1.063	"
	280	19.0	667	940	1.064	"
	240	16.3	669	942	1.062	"
	210	14.3	667.5	940.5	1.063	"
	Hg _{.52} Te _{.48}	565	38.4	813	1086	0.921
460		31.3	780	1053	0.950	"
395		26.9	756	1029	0.972	"
350		23.8	734	1007	0.993	"
305		20.75	713	986	1.014	"
270		18.4	692	965	1.036	"
245		16.7	675	948	1.055	"
243		16.5	664	937	1.067	"
280		19.0	663	936	1.068	Liquidus Arrest
270		18.4	656	929	1.076	"
Hg _{.60} Te _{.40}	380	25.9	704	977	1.024	Melt P-T
	320	21.8	678	951	1.05	"
	285	19.4	662	935	1.07	"

(Cont.)

TABLE III (Cont.)

Composition	Pressure		Temperature		$\frac{10^3}{T}$	Effect
	psi	atm	°C	K		
Hg _{.70} Te _{.30}	282	19.2	656	929	1.078	Melt P-T
	410	27.9	656	929	1.077	Liquidus Arrest
	365	24.8	656	929	1.077	"
	350	23.8	656	929	1.077	"
	330	22.4	656	929	1.077	"
	310	21.1	656	929	1.077	"
	275	18.7	656	929	1.077	"
	433	29.5	690	963	1.038	Melt P-T
	265	18.0	629	902	1.109	"
	365	24.8	629	902	1.109	Liquidus Arrest
	330	22.4	629	902	1.109	"
	305	20.7	629	902	1.109	"
	270	18.4	629	902	1.109	"
	265	18.0	629	902	1.109	"

pseudobinary $\text{Hg}_{.70}\text{Cd}_{.30}\text{-Te}$ system (Table IV). The experimented data is plotted in Figure 13 on a $\ln P$ vs. $1/T$ plot.

Over the range of 9 to 98 atmospheres, the experimental data gives

$$\ln P_{\text{atm}} = 11.27 - \frac{7,160}{T} \quad (1)$$

or

$$\log P_{\text{atm}} = 4.894 - \frac{3,109}{T} \quad (1')$$

The pressure-temperature curves over the binary Hg-Te melts also form approximately linear straight lines with slopes parallel to that of pure Hg . The liquidus temperature obtained for stoichiometric HgTe is $669 \pm 2^\circ\text{C}$. The liquidus pressure increases from 16 ± 1 atm. for stoichiometric HgTe to a maximum of 19 atm. for the composition $\text{Hg}_{.60}\text{Te}_{.40}$.

Similar pressure-temperature curves have also been obtained over ternary $\text{Hg}_{.70}\text{Cd}_{.30}\text{-Te}$ melts but in a much higher pressure range. The maximum liquidus temperature determined for $\text{Hg}_{.70}\text{Cd}_{.30}\text{Te}$ is $850 \pm 2^\circ\text{C}$. The pressure along the liquidus increases from 44 atm. to a maximum of about 72 atm. for the composition $(\text{Hg}_{.70}\text{Cd}_{.30})_{.60}\text{Te}_{.40}$. The solidus temperature for the pseudobinary composition $\text{Hg}_{.70}\text{Cd}_{.30}\text{Te}$ is 727°C (Figure 14).

E. EVALUATION OF RESULTS

The data shown in Table II for the vapor pressure of pure Hg is in very good agreement with the high pressure data of Cailletet et al⁽⁸⁾ dating back to 1900 and reported in⁽⁹⁾. Equation (1') representing our data also compares well with the expression for lower pressures given by⁽¹⁰⁾:

$$\log P_{\text{atm}} = 4.891 - \frac{3.08 \times 10^3}{T} \quad (2)$$

over the range of 333 to 567°C .

TABLE IV

Pressure-Temperature Data
for the
Hg_{.70}Cd_{.30}-Te System

Composition	Pressure		Temperature		$\frac{10^3}{T}$	Effect
	psi	atm	°C	K		
(Hg _{.70} Cd _{.30}) _{.50} Te _{.50}	780	53.1	889	1162	0.861	Melt P-T
	720	49.0	877	1150	0.869	"
	720	49.0	876	1149	0.870	"
	720	49.0	875	1148	0.871	"
	643	43.75	854	1127	0.887	"
	593	40.3	835	1108	0.903	"
	685	46.6	852	1125	0.889	Liquidus Arrest
	650	44.2	849	1127	0.891	"
	-	-	727	1000	1.000	Solidus Arrest
(Hg _{.70} Cd _{.30}) _{.60} Te _{.40}	1100	74.8	825	1098	0.911	Melt P-T
	1030	70.1	817	1090	0.917	"
	980	66.7	801	1074	0.931	"
	1050	71.4	818	1091	0.917	Liquidus Arrest
(Hg _{.70} Cd _{.30}) _{.70} Te _{.30}	1305	88.8	827	1100	0.909	Melt P-T
	1300	88.4	825	1098	0.911	"
	1133	77.1	799	1072	0.933	"
	1030	70.0	776	1049	0.954	"
	970	66.0	748	1021	0.978	"
	770	52.4	709	982	1.018	"
	647	44.1	694	967	1.034	"
	1070	72.8	749	1022	0.978	Liquidus Arrest
	1040	70.7	778	1051	0.951	"

(Cont.)

TABLE IV (Cont.)

Composition	Pressure		Temperature		$\frac{10^3}{T}$	Effect
	psi	atm	°C	K		
(Hg _{.70} Cd _{.30}) _{.40} Te _{.60}	665	45.2	939	1212	0.824	Melt P-T
	544	37.0	917	1190	0.840	"
	460	31.3	891	1164	0.858	"
	350	23.8	851	1124	0.889	"
	280	21.0	813	1086	0.922	"
	230	15.6	780	1073	0.948	"
	165	11.2	733	1006	0.995	"
	-	-	779	1052	0.950	Liquidus Arrest

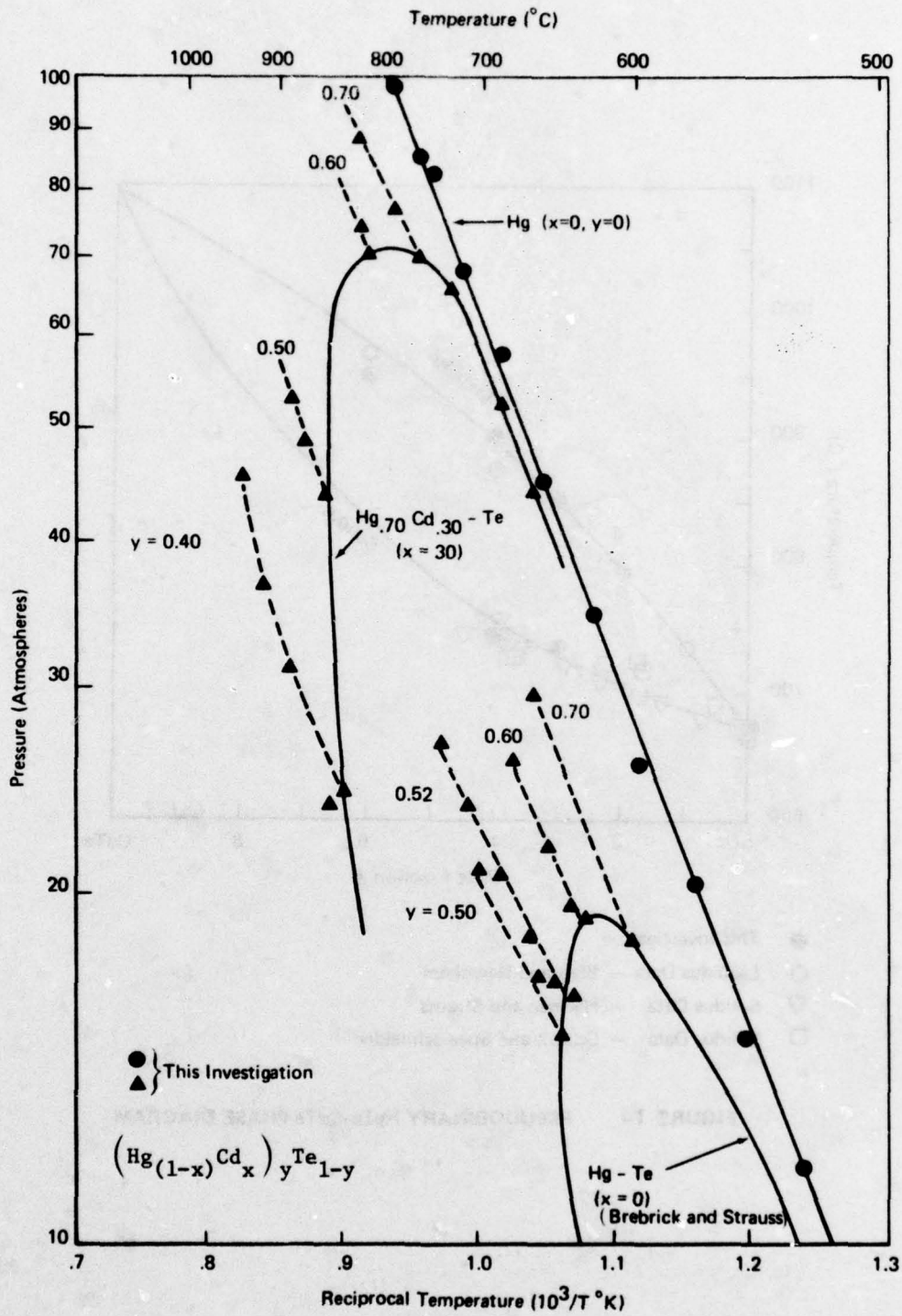
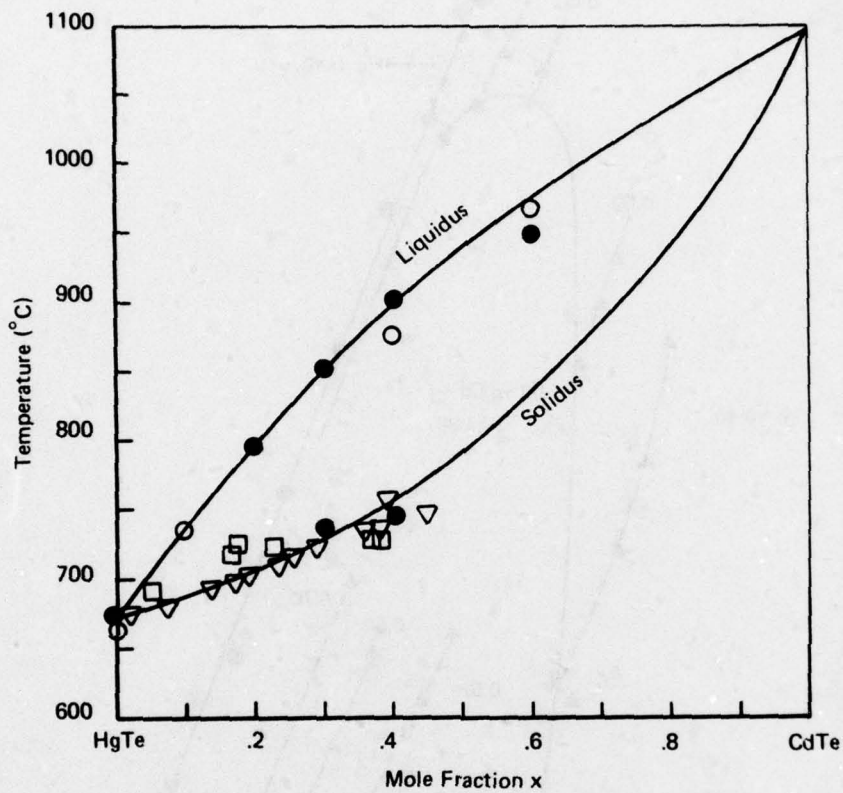


FIGURE 13 Hg-Cd-Te PRESSURE-TEMPERATURE PHASE DIAGRAM



- This Investigation
- Liquidus Data - Blair and Newnham
- ▽ Solidus Data - Harman and Strauss
- Solidus Data - Schmit and Speerschneider

FIGURE 14 PSEUDOBINARY HgTe-CdTe PHASE DIAGRAM

By derivation from the Clausius-Clapeyron equation, one can write:

$$\ln P = - \frac{\Delta H_v}{RT} + c \quad (3)$$

with ΔH_v : heat of vaporization

R : ideal gas constant = $1.98 \text{ cal}^\circ\text{K}^{-1} \text{ mole}^{-1}$

c : integration constant.

Equation (1) then yields for the heat of vaporization of pure Hg:

$$\Delta H_v = 14.175 \text{ kcal/g-at} \quad (4)$$

which compares with the literature value⁽¹¹⁾ of 13.985 kcal/g-at at 356°C and 1 atmosphere.

Because of the interest in HgCdTe detector material, the ternary Hg-Cd-Te phase diagram has been the subject of several prior investigations. These have been mostly concentrated in the low temperature-low pressure regions of the diagram. The pseudobinary HgTe-CdTe liquidus and solidus curves have been investigated by thermal analysis^(3, 12, 13) and by determination of segregation coefficients from solidification profiles.⁽¹⁰⁾ A large portion of this data is of limited value however since the vapor pressure over the charge was not determined. The importance of the pressure has been shown by the work of Brebrick and Strauss⁽¹⁰⁾ on the determination of the pressure-temperature (P-T) phase diagram of the binary Hg-Te system. (Their liquidus curve is shown in Figure 13.) This was done by spectrometric analysis of the vapor in equilibrium with the condensed phases, melt or liquid-solid compositions corresponding to the liquidus-solidus equilibrium. Schmit and Speerschneider⁽¹⁴⁾ also investigated the P-T diagram of the pseudobinary $\text{Hg}_{.80}\text{Cd}_{.20}\text{-Te}$ cross-section by thermal analysis in sealed ampoules containing a reservoir of Hg. By controlling the temperature of the reservoir, the Hg vapor pressure could be adjusted within a broad range. The difficulty with this technique, however, is in the interpretation of the thermal arrests obtained under controlled pressure. In

contrast with the method of Brebrick and Strauss, it is difficult to determine if these correspond to actual three-phase equilibrium conditions.

The liquidus-solidus equilibrium P-T curve for the binary system Hg-Te obtained by Brebrick and Strauss is reproduced on Figure 13. It can be seen that the agreement with our high pressure furnace data is very good. This indicates that, within experimental error, the pressure of inert gas determined by the pressure balancing technique corresponds to the vapor pressure of Hg determined by other techniques, such as vapor phase spectrography.

There has been no previous investigation of the P-T curve for the system $\text{Hg}_{.70}\text{Cd}_{.30}\text{-Te}$. Only the pseudobinary liquidus and solidus temperatures have been determined by thermal analysis in sealed quartz ampoules. Our liquidus data (Figure 14) shows a higher temperature than those obtained in the previous investigations^(3, 13) because of the higher vapor pressure. Our solidus temperature, however, is in good agreement with the data of⁽¹²⁾ calculated from segregation coefficients, while that of⁽¹⁴⁾ shows more scatter on either side of the curve.

SECTION IV
MATERIALS PREPARATION

The results from preliminary crystal growth experiments stressed the need to optimize the growth procedure before meaningful thermodynamic measurements could be made. More than 30 preparations were made before we achieved this goal. Details of our approach are set out below.

Preparation 47 ($x = 0.3$)

The ingot derived from preparation 47 was sliced in the manner shown in Figure 15. The bottom of the ingot was sliced as horizontal wafers; the next 10 millimeter section was sliced parallel to the principal axis (A); the upper section of the ingot was then cut into two halves parallel to the major axis; one-half was then cut into vertical planks (B), and the other into horizontal semicircles (C). The measured densities are listed in Tables V and VI.

The solidification procedure was a two-step process, with initial rapid lowering over the first 1 1/2", followed by slower lowering over the remaining 1 1/2". It is apparent from the densities that the solidification was not fast enough to prevent wide variation in x values ranging from $x = 0.269$ to 0.476 . The two-step solidification masks any trend in temperature gradient except in the radial profile deduced from the A series; the low serial number side would appear to be colder. We were unable to identify a liquidus arrest in the cooling curve.

Preparation 48 ($x = 0.3$)

In preparation 48, the ampoule was initially lowered at 0.1"/min for 13.5 min. then at 4"/min for 32 sec. The objective was to generate large grains in the bottom of the ampoule to provide nucleation for the subsequent fast solidification. This ingot was broken by a thermocouple probe during profiling immediately after solidification. However, three large pieces were retrieved. Density measurements were possible for three horizontal wafers

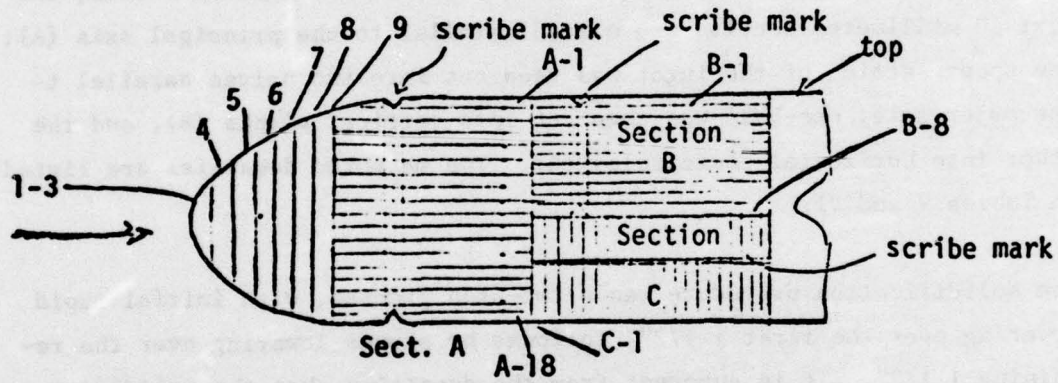


FIGURE 15 METHOD OF SLICING INGOT 47

Table V
Densities and X Values for Vertical Slices of Preparation 47

	Density g/cm ³	x
A1	6.941	0.510
A2	7.016	0.476
A3	7.075	0.449
A4	7.186	0.399
A5	7.269	0.362
A6	7.334	0.333
A7	7.343	0.306
A8	7.436	0.288
A9	7.470	0.272
A10	7.476	0.269
A11	7.462	0.275
A12	7.463	0.275
A13	7.452	0.280
A14	7.440	0.285
A15	7.419	0.295
A16	7.413	0.298
A17	7.403	0.302
A18	7.388	0.309

Table VI

Densities and X Values for Sections B and C of Preparation 47

	<u>Density g/cm³</u>	<u>X</u>
B1	7.254	0.369
B2	7.266	0.364
B3	7.275	0.360
B4	7.291	0.353
B5	7.296	0.350
B6	7.312	0.343
B7	7.353	0.325
B8	7.430	0.292
C1	7.255	0.369
C2	7.289	0.353
C3	7.329	0.335
C4	7.356	0.323
C5	7.366	0.319
C6	7.373	0.316
C7	7.371	0.316
C8	7.382	0.312
C9	7.384	0.311
C10	7.376	0.314
C11	7.357	0.323
C12	7.338	0.331
C13	7.307	0.345

at the equivalent of slices 9, 20, and 27 of a complete ingot. The apparent x values were 0.236, 0.343 and 0.351 respectively, with the last value being closest physically to the thermocouple. A thermal arrest was observed at 870°C -- a figure which corresponds quite closely with the liquidus temperature for an x value of 0.351. However, since we do not know when the thermocouple begins to respond to the freezing process, it is important to improve on the uniformity of x values through the melt if we are to make a confident correlation between the liquidus temperature and composition.

Preparation 49 (x = 0.3)

The solidification procedure in this preparation involved the single step of lowering the ampoule at 1/2"/min. An attempt was made to reheat the ampoule for limited recrystallization, but a delay in returning the power to the furnace resulted in a thermal shock which cracked the ampoule. The ingot was undamaged, and again three slices corresponding to 9, 20 and 27 in a complete analysis were cut and the density determinations made. The x values derived were 0.351, 0.366 and 0.381 respectively. A liquidus arrest was observed at 852°C -- a result somewhat at variance with preparation 48 and probably too low to correspond to the measured x value of 0.381.

Preparation 51 (x = 0.2)

As indicated earlier, studies under another program suggested that there might be a problem in obtaining homogeneity in the liquid phase with high x values of $\text{Hg}_{1-x}\text{Cd}_x\text{Te}$. (For example, in preparation 50, which was an x = 0.45 run, the measured x values ranged from 0.26 at slice 9 to 0.65 at the top of the ingot.) For this reason, it was decided to establish our experimental method for x = 0.2 which presents a lesser problem in liquid phase homogeneity. In preparation 51, we set out to check on this by solidifying as rapidly as possible. Despite the fact that this procedure was expected to destroy the ampoule, it survived the cool-down. and very little coring of the ingot occurred. Unfortunately, a problem with the thermocouple prevented the measurement of a thermal arrest. The density data listed in Table V showed remarkable uniformity; slices 9,

20 and 29 all showed a density of 0.209; the data for vertical planks between slices 23 and 29 showed only a slight decrease towards the center. A double thickness wafer cut into quadrants (A,B,C, and D) showed no radial distribution in x.

Preparation 52 (x = 0.2)

This preparation was a duplicate of 51 and generated uniform x values which compared favorably with it, but the value, typically 0.225, was higher, indicating that we were unable to reproduce the conditions exactly. A thermal arrest was observed at 785°C -- a figure which is a little lower than that normally accepted for x = 0.22.

Preparations 53 and 54 (x = 0.45)

These preparations were of x = 0.45 material for the preparation of photovoltaic devices for another program.

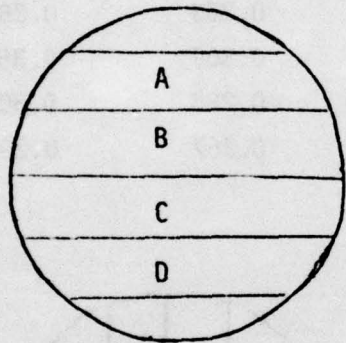
Preparations 55 and 56 (x = 0.2)

In these preparations we examined the characteristics of crystals prepared by very slow solidification to look at the specific differences between fast and slow cooling. Preparation 55 was solidified by slowly lowering the furnace power over a period of three days. The lower half of the crystal consisted of two grains. The upper section was composed of a larger number of medium size grains. The homogeneity, defined by density measurements, yielded x values of 0.211, 0.212 and 0.198 for slices 9, 19 and 20 respectively. However, bars cut orthogonally from slices 19 and 20 showed significant variation in x. Similar variations may be observed in vertical planks cut between slices 10 and 19. These data are presented in Table VII. A similar pattern was observed with preparation 56 which was solidified by slow lowering of the ampoule over two days. Slices 10, 19 and 29 had x values of 0.270, 0.270 and 0.252 respectively. But, as shown in Table VIII, the segments of slices 9, 10, 28 and 29 showed considerable variation in x.

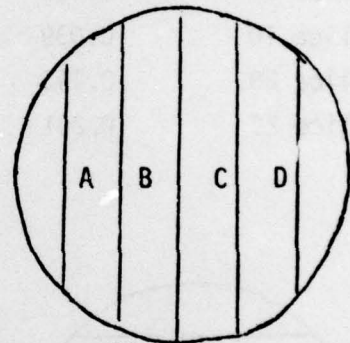
Table VII

DENSITY VALUES FOR CRYSTAL 56

	A	B	C	D
Slice 19	0.165	0.210	0.239	0.293
Slice 20	0.341	0.267	0.140	0.060



Slice 19



Slice 20

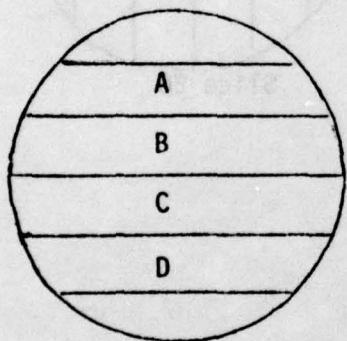
Planks between slices 10 and 19

- 1. 0.329
- 2. 0.327
- 3. 0.316
- 4. 0.316
- 5. 0.313
- 6. 0.315
- 7. 0.289
- 8. 0.276
- 9. 0.260
- 10. 0.238
- 11. 0.196
- 12. 0.160
- 13. 0.130

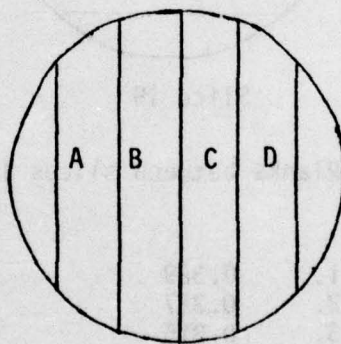
Table VIII

DENSITY VALUES FOR CRYSTAL 55

Slice 9	0.185	0.198	0.263	0.289
Slice 10	0.039	0.141	0.309	0.351
Slice 28	0.143	0.242	0.285	0.301
Slice 29	0.201	0.267	0.267	0.235



9 and 28



10 and 29

We may conclude that we have a temperature gradient across the diameter of the ampoule, and this gradient is not linear nor is it consistent along the length of the crystal; i.e., we could not cut plane slices of uniform composition of any significant size from these crystals.

Preparations 57 and 58 (x = 0.2)

The high pressure furnace was modified by placing heat reflecting shields in the lower region of the furnace. The objective was to impose a uniform horizontal temperature profile through which the ampoule could be lowered. The vertical profile was arranged such that above the reflecting shield the temperature was above the liquidus and below the shield was below the solidus temperature. Crystal 57 was obtained by slow lowering. The bottom of the crystal was single with one large mercury pit; the top consisted of a few large grains. The densities recorded in Table IX show that we were not successful in eliminating the radial temperature gradient. Preparation 58 was a smaller ampoule but was solidified in an identical manner to 57. It was small grained and extensively cracked and was not subject to any characterization tests.

Preparations 59 and 60 (x = 0.2)

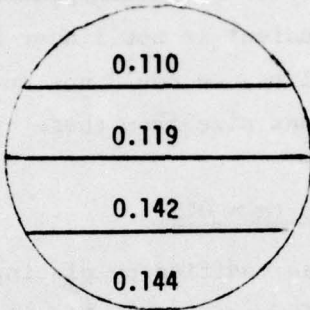
These crystals were prepared in the same manner as crystals 57 and 58; i.e., slow lowering. The one difference was that the ampoules were sharply pointed at the base instead of being hemispherical. Neither run was successful since both crystals were polycrystalline and extensively cracked. This was considered to be due to degradation of the heat shield so that both crystals were exposed to a steep thermal gradient for an extended period of time, and this caused the cracking.

Preparation 61 (x = 0.2)

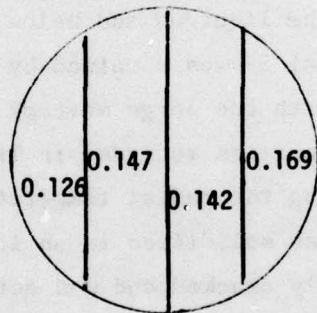
Since we knew that the horizontal temperature profile of the furnace was not flat, we attempted in this preparation to induce crystallization in a horizontal plane. The bottom half of the crystal was single and again the top consisted of a few large grains. From the x values obtained for slices

Table IX
BAR DENSITIES FOR SLICES 20,21,42 AND 43
FOR CRYSTAL 57

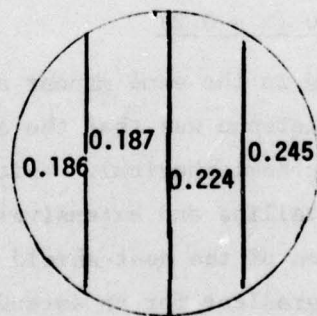
SLICE 43



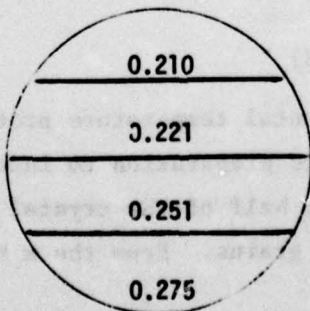
SLICE 42



SLICE 21



SLICE 20



10, 11, 29, 30, 47 and 48, see Table X, it would appear that we obtained simultaneous freezing from the top and the bottom. This is confirmed by the orthogonal bar densities determined for slices 10 and 11 as shown in Table XI. This approach was not pursued.

Preparation 62 (x = 0.2)

The solidification procedure involved powering down the furnace from 780°C to 685°C over a six-hour period after which the ampoule was held at 680°C for nearly four days. The ingot was single crystal for the lower third. The top was composed of some seven or eight large grains. The density data are given in Table XII. The figures demonstrate that we did achieve directional axial freezing, but the freezing interface was not planar nor perpendicular to the direction of growth. In contrast to previous preparations, this material was p type as grown.

Preparation 63 (x = 0.2)

In this preparation a sealed ampoule was used to check the influence of possible impurities on the electronic properties of the as grown crystals. We were particularly concerned about the presence of oxygen. Because the ampoule was sealed a lesser amount of excess mercury was used; nevertheless because the neck of the ampoule was cool a significant quantity of mercury was in reflux. The result was a spongy cored crystal which was not characterized.

Preparation 64 (x = 0.2)

This crystal was solidified by rapid quenching under low mercury vapor pressure conditions. A furnace leak required an emergency shut down and during the rapid cooling the crystal was destroyed by cracking.

Preparations 65 and 66 (x = 0.2)

A water cooled heat sink was used to initiate solidification. From past experience we expected a polycrystalline ingot of uniform x value. In preparation 65 after solidification the temperature was raised to 727°C

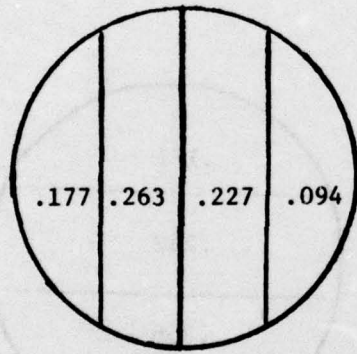
Table X

DENSITIES AND X VALUES FOR CRYSTAL 61

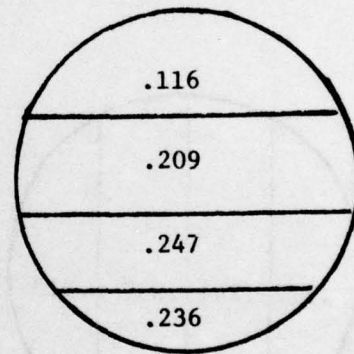
Slice	ρ g/cm ³	x
10	7.62	0.206
11	7.61	0.209
29	7.72	0.160
30	7.71	0.165
47	7.50	0.259
48	7.49	0.265

Table XI

ORTHOGONAL BAR DENSITIES OF SLICES 10 AND 11
FOR CRYSTAL 61



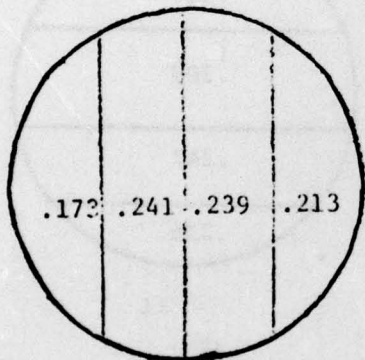
10



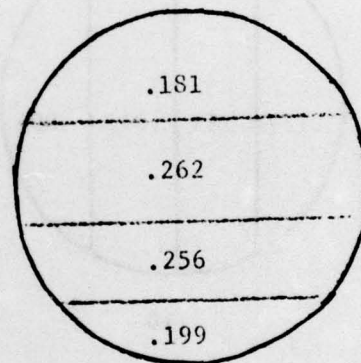
11

Table XII

ORTHOGONAL BAR DENSITIES OF SLICES 9 AND 10
OF CRYSTAL 62



9



10

to effect partial melting. A second solidification was then carried out by cooling to 690°C over a period of sixteen hours. The central region had large grains with x values close to 0.23. The lower region was polycrystalline. The top of the crystal had decomposed.

For preparation 66 the raise in temperature after solidification was to 710°C for ten hours. The ingot was then held at 690°C for fourteen days. The lower half of the ingot was still polycrystalline with large grains in the upper half. The x values in the upper half ranged from 0.226 to 0.210.

Preparations 67 and 68 (x = 0.2)

Both these preparations were carried out before it was realized that the heat pipe was not functioning due to the uptake of hydrogen. The hydrogen which is produced by reaction of trace quantities of water with the carbon resistance heater diffuses through Inconel walls of the heat pipe and depresses the vaporization of sodium. It was regenerated by baking in vacuum.

Preparations 69 and 70 (x = 0.2)

These preparations were solidified by identical fast quench procedures. One ingot was recrystallized in the high pressure furnace, the second in a sealed ampoule in a separate furnace with a flat temperature profile. This approach followed a pattern established in a parallel series of experiments described below in which pieces of ingot 51 (uniform x but very polycrystalline) were successfully converted to single crystals.

In this case the ampoule exploded in the recrystallization step. The ingot recrystallized in the high pressure furnace remained polycrystalline.

Preparation 71 (x = 0.2)

A rapidly solidified ingot, formulated to have an x value of 0.2, was recrystallized in a sealed quartz ampoule which also contained a portion of the ingot crushed to a fine powder to provide a mercury vapor pressure corresponding to that of the ingot. This prevented decomposition of the ingot,

since the powder was maintained at a slightly higher temperature. We obtained a crystal with several large grains with x values ranging from 0.201 to 0.209.

Preparations R1-R6 (x = 0.2)

Because of the acknowledged inhomogeneous temperature profile of the high pressure furnace we adopted as standard procedure (Series R) rapid solidification in the high pressure furnace followed by recrystallization in a sealed ampoule in a separate flat profile furnace. At the completion of the contractual effort we had established a procedure for rapid solidification, in the high pressure furnace, with subsequent conversion to large grained or single crystal material in sealed quartz ampoules. In the last sample to be characterized the x values ranged from 0.186 to 0.206 in a quadrant cut from a half-inch diameter ingot one inch in length. After annealing, carried out during report preparation, carrier concentrations of better than $10^{15}/\text{cm}^3$ were observed.

Comments on Revised Recrystallization Procedure

From the point in the program when preparation 61 was made we started a parallel program to examine the possibility of recrystallization of polycrystalline ingots of uniform x composition in a furnace with an established flat temperature profile. The basis of this approach was that we could retain the additional degree of freedom; i.e., mercury vapor pressure control, associated with the high pressure furnace. At the same time by cutting the ingot and powdering part of it, and including this powder in the sealed quartz ampoule at a slightly elevated temperature, we carried out the recrystallization step under controlled conditions. All the characterization experiments carried out indicate that this is a preferred method of approach. Carrier concentrations were measured at less than $10^{15}/\text{cm}^3$ with x values ranging in a single ingot from 0.186 to 0.206.

SECTION V

DISCUSSION

The experimental program described in the previous sections serves to emphasize the experimental difficulties associated with the preparation of large grained crystals of mercury cadmium telluride in the high pressure furnace. At its conclusion, we had defined a viable method for producing uniform material with acceptable electronic properties. This method retains the advantages of the high pressure furnace for compounding large diameter ingots under circumstances in which the mercury vapor pressure can be varied. In order to obtain uniform material it is necessary to solidify the charge very rapidly, i.e., the temperature gradient to which the charge is subjected is so large that poorly controlled temperature profile inherent in the high pressure furnace is of little influence. For this same reason the polycrystalline material produced by the rapid solidification had to be recrystallized in a sealed ampoule in a furnace with a well controlled temperature profile. As stated before, by powdering a portion of the ingot we maintained the equilibrium mercury vapor pressure above the ingot at a value that corresponded to the conditions during solidification. By this approach we have met the initial objectives of the program. However other than the vapor pressure-temperature relationships reported here we have had no opportunity to make thermodynamic determinations relevant to the phase diagram, such as the solidus and liquidus points pertaining to the HgCdTe phase, since we did not succeed in manufacturing material of well defined uniform composition until the very last stages of the program. Note that there is a significant difference between the small samples required for detector fabrication and the larger quantities of material required for thermodynamic determinations.

SECTION VI

REFERENCES

1. J. Steininger, J. Electronic Materials, 5, 299 (1976).
2. W.D. Lawson, S. Nielson, E.H. Putley and A.S. Young, J. Phys. Chem. Solids, 9, 325 (1959).
3. J. Blair and R. Newnham, "Metallurgy of Elemental and Compound Semiconductors," Interscience, 12, 393 (1961).
4. J. Steininger, J. Appl. Phys., 41, No. 6, 2713-2727 (1970).
5. J. Steininger and A.J. Strauss, J. Crystal Growth, 13/14, 657-662 (1972).
6. J. Steininger, J.F. Butler and J. Sohn, Proc. Spec. Meeting on Physics of Detectors, Orlando, Florida, 135-143 (1972).
7. J. Steininger, Alan J. Strauss and R.F. Brebrick, J. Electrochem. Soc., 117, No. 10, 1305-1309 (1970).
8. L. Cailletet, E. Collardeau and C.A. Riviere, Compt. Rend., 130, 1585 (1900).
9. A.N. Nesmeyanov, Vapor Pressure of the Chemical Elements, Elsevier Co., New York (1962).
10. R.F. Brebrick and A.J. Strauss. J. Phys. Chem. Solids, 26, 989 (1965).
11. Handbook of Physics and Chemistry, 51st ed., R.C. Weast, ed., D-56, The Chemical Rubber Co., Cleveland, Ohio (1970).
12. T.C. Harman in Physics and Chemistry of II-IV Compounds, M. Aven and J.S. Prener, eds., p. 784, Wiley (Interscience), New York (1967).
13. B. Ray and P.M. Spencer, Phy. Status. Solidi, 22, 371 (1967).
14. J.L. Schmit and C.J. Speerscheider, Infrared Phys., 8, 247 (1968).

FILM
4